

Vector Magnetometer Using Rb Vapor

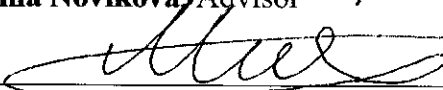
A thesis submitted in partial fulfillment of the requirement
for the degree of Bachelors of Science in Physics from
The College of William and Mary

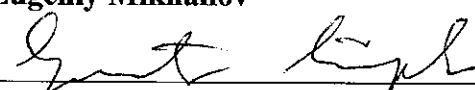
by

Kevin Cox

Accepted for Honors
(Honors, No Honors)


Irina Novikova, Advisor


Eugeny Mikhailov


Gunter Luepke


Charles Perdrisat, Director

Williamsburg, VA
April 25, 2011

Vector Magnetometer Using Rb Vapor

Kevin Cox

May 3, 2011

Abstract

This project demonstrates an optical method for measuring the strength and direction of a magnetic field using electromagnetically induced transparency (EIT) in rubidium vapor. In rubidium atoms, the Zeeman effect causes atomic states to shift when an external magnetic field is applied. The magnitude of these shifts, and consequently the strength of the magnetic field, can be measured by recording electromagnetically induced transparency resonances with tuned laser fields. Furthermore, since the atom's interaction with the laser field is dependent on the direction of the magnetic field and the laser polarization, we are able to determine the direction as well as the strength of the magnetic field by analyzing relative intensities of EIT resonances. With a feasible precision down to 10 picoTesla and the possibility of complete field mapping, this magnetometer can be useful for medical, geophysical, and materials testing applications.

1 Introduction

Classical magnetometers such as Hall probes and fluxgate magnetometers, have a fruitful history in the fields of geosensing and navigation, but over the past 50 years, researchers have studied how atomic and quantum mechanical phenomena sensitive

to magnetic fields can be measured. These new techniques have pushed the sensitivity of magnetometers down by many orders of magnitude making them vitally important in precision materials testing and medical imaging. Figure 1 below shows the scales of common magnetic fields and the sensitivity of magnetometers. This figure shows the tremendous leaps in magnetometer technology in the last century. The fluxgate magnetometer was state of the art in the 1930's. Now, the SQUID magnetometer and the EIT magnetometer presented in this thesis are five orders of magnitude more sensitive.

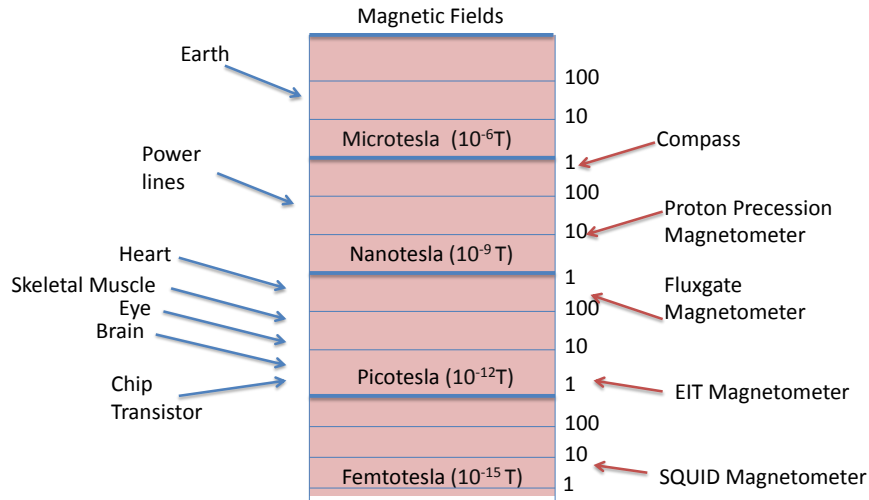


Figure 1: Common magnetic field strengths and magnetometer sensitivities.

Currently, one of the most glamorous of sensitive magnetometers, the superconducting quantum interference device (SQUID) [1] can measure the magnitude of magnetic fields down to 1fT. The SQUID is being used at Los Alamos National Lab to measure the magnetic fields of the brain (below 1pT), treating seizure patients and measuring fetal heartbeats. Yet, this wonderful device still has several drawbacks. In order to measure the minute fields from human organs, the device must be positioned close to the human body. However, since the SQUID is a superconducting

device, it must be cooled to below 100K. To solve the problem, researchers engineered a superconducting helmet which houses many SQUID magnetometers to image the brain's fields. By necessity this helmet is large and expensive. Additionally, the SQUID can only measure the strength of magnetic fields, allowing information about the directionality of brain (and other organs) currents to be overlooked. In fact, to my knowledge, no magnetometer has been developed which can measure the strength and direction of brain electromagnetic activity.

While the SQUID is the most sensitive magnetometer in commercial operation today, able to measure magnetic fields with 10^{-15} Tesla precision, atomic magnetometers are being developed with comparable or better sensitivity which are much more compact and economical to build [3]. Ten years ago, researchers at Princeton developed an atomic magnetometer capable of measuring small magnetic fields with a proposed precision of 10^{-16} Tesla [2]. This magnetometer, like the magnetometer which I will be presenting in this thesis, uses vaporous Rb in a glass cell. In order to measure the strength of the magnetic field, this Spin Exchange Relaxation Free (SERF) magnetometer limits the ability of the rubidium atoms to lose their spin polarization as a result of atomic collisions within the gas cell. Then, the precession of the spin polarized atoms in the magnetic field can be measured. The SERF has one significant drawback. Although the SERF has a sensitivity of 10^{-16} Tesla, this sensitivity is only achievable around a zero magnetic field. This limits the use of the magnetometer for many commercially useful situations.

In this project, we have developed another type of atomic magnetometer which relies on an effect called electromagnetically induced transparency (EIT) in rubidium vapor to measure magnetic fields. EIT is an effect which causes a three-level quantum mechanical system, when addressed by two properly tuned laser fields, to become relatively transparent. This effect allows precise spectroscopy of Rb atomic sublevels from which the magnetic field can be deduced (and can also be useful for

atomic clocks) [5]. Furthermore, the EIT magnetometer presented in this thesis has the capability of addressing several of the limitations of the SQUID and SERF magnetometers and can feasibly measure magnetic fields with a sensitivity of 10 pT, beneath that required to measure fields from the human heart and brain. One of the main thrusts of my thesis work is to prove that the EIT magnetometer is capable of measuring magnetic field direction as well as strength, leading to the possibility of complete spatial magnetic vector field maps. For this reason, the EIT magnetometer has the capability of finding a purpose for navigation, medical measurements, and possibly materials testing which other mainstream magnetometers such as the SERF magnetometer and the SQUID cannot fulfill.

2 Theory

2.1 Rb in a Magnetic Field

There are two main ways in which rubidium atoms respond to a magnetic field. The first is the Zeeman effect; the shifting of atomic energy levels in the presence of a magnetic field. The Zeeman effect is sensitive to the magnitude of the magnetic field, and for rubidium 87 on the D1 line this effect has a magnitude of

$$\Delta f = m \cdot g \cdot \mu_B \cdot B \quad (1)$$

where m is the z -direction of angular momentum quantum number, g is the gyromagnetic ratio and μ_B is the Bohr magneton with $\mu_B \cdot g = m \cdot (.7 \text{ MHz/G})$ for ^{87}Rb used in our experiments. The second effect is the quantization of the magnetic dipole moment of the atom in the direction of the magnetic field. This means we allow the magnetic field to specify the z -direction (projection direction of m) of the atoms and determine how light of different polarizations interact with the atoms. If we can

measure both of these effects, the energy level splitting due to the zeeman effect and the projection direction of $|m\rangle$, the entire magnetic field's magnitude and direction will be known. We use electromagnetically induced transparency to gain access to this information. In the EIT magnetometer, EIT doesn't directly measure magnetic fields. The Rb atoms measure the field, then EIT measures the energy levels and orientation of the Rb atom.

2.2 Electromagnetically Induced Transparency

As the name implies, EIT refers to the ability of an atom or group of atoms to become relatively transparent when electromagnetic fields are applied in a proper way. EIT occurs in a three-level quantum system as shown below in figure 2. When two laser fields are tuned to transitions from two ground states, labeled $|b\rangle$ and $|c\rangle$, to an excited state, labeled a , atoms are pumped into a new noninteracting state, causing the medium to become transparent.

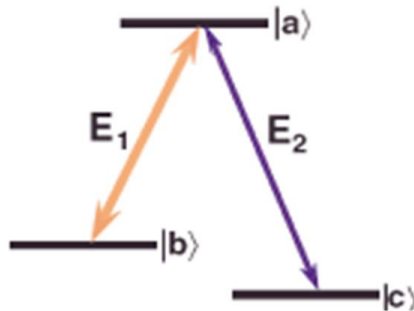


Figure 2: Three-level Λ -system. States $|c\rangle$ and $|b\rangle$ are ground states coupled to the excited state, $|a\rangle$, with two laser fields, E_1 and E_2 .

The exact theoretical calculations of EIT resonances in ^{87}Rb vapor done in conjunction with this experiment are complicated, and were carried out using the density matrix formalism method by our theoretical collaborators at Novibisirsk, Russia [6]. However, it is useful to overview the basics of EIT, from a simple quantum mechanics

perspective which can illustrate all of the main aspects of the EIT magnetometer. For EIT we use time dependent perturbation theory to solve the three-level system which can be written out as shown below [7]. c_a , c_b , and c_c are time dependent population densities of the states $|a\rangle$, $|b\rangle$, and $|c\rangle$.

$$\Psi = c_a(t)\psi_a e^{-iE_a t/\hbar} + c_b(t)\psi_b e^{-iE_b t/\hbar} + c_c(t)\psi_c e^{-iE_c t/\hbar} \quad (2)$$

We need to solve the time-dependent Schrödinger equation for this system,

$$H\Psi = i\hbar \frac{\partial \Psi}{\partial t} \quad (3)$$

with $H = H^0 + H'$, where H^0 is the initial atomic Hamiltonian of the system and H' is the perturbed Hamiltonian describing the effect of the electromagnetic fields. Time dependent perturbation theory gives us the matrix equation,

$$\begin{pmatrix} H'_{aa} & H'_{ab} & H'_{ac} \\ H'_{ba} & H'_{bb} & H'_{bc} \\ H'_{ca} & H'_{cb} & H'_{cc} \end{pmatrix} \begin{pmatrix} c_a e^{-iE_a t/\hbar} \\ c_b e^{-iE_b t/\hbar} \\ c_c e^{-iE_c t/\hbar} \end{pmatrix} = i\hbar \frac{\partial}{\partial t} \begin{pmatrix} c_a e^{-iE_a t/\hbar} \\ c_b e^{-iE_b t/\hbar} \\ c_c e^{-iE_c t/\hbar} \end{pmatrix} \quad (4)$$

where H'_{ij} is the matrix element $\langle \psi_i | H' | \psi_j \rangle$. We consider two laser fields are applied to the atom in the configuration shown in figure 2. In that case, we can assume that the laser field E_1 only interacts with states ψ_a and ψ_b while laser field E_2 interacts with only ψ_a and ψ_c . This means $H'_{bc} = H'_{cb} = 0$. Furthermore, the matrix elements H'_{aa} , H'_{bb} , and H'_{cc} evaluate to zero, and $H'_{ab} = \hbar\Omega_1 e^{-i\omega t}$, $H'_{ac} = \hbar\Omega_2 e^{-i\omega t}$ where Ω_1 and Ω_2 are the Rabi frequencies of oscillations for the transitions $|a\rangle - |c\rangle$ and $|a\rangle - |b\rangle$ respectively. Now, we rewrite the matrix equation,

$$\begin{pmatrix} 0 & \hbar\Omega_1 e^{i\omega_1 t} & \hbar\Omega_2 e^{i\omega_2 t} \\ \hbar\Omega_1 e^{-i\omega_1 t} & 0 & 0 \\ \hbar\Omega_2 e^{-i\omega_2 t} & 0 & 0 \end{pmatrix} \begin{pmatrix} c_a e^{-i\omega_a t} \\ c_b e^{-i\omega_b t} \\ c_c e^{-i\omega_c t} \end{pmatrix} = i\hbar \begin{pmatrix} \frac{\partial}{\partial t} c_a e^{-i\omega_a t} \\ \frac{\partial}{\partial t} c_b e^{-i\omega_b t} \\ \frac{\partial}{\partial t} c_c e^{-i\omega_c t} \end{pmatrix} \quad (5)$$

Written out, the equations are,

$$i\dot{c}_a = \Omega_1 e^{i(\omega_1 - \omega_{ab})t} c_b + \Omega_2 e^{i(\omega_2 - \omega_{ac})t} c_c \quad (6)$$

$$i\dot{c}_b = \Omega_1 e^{i(\omega_2 - \omega_{ab})t} c_a \quad (7)$$

$$i\dot{c}_c = \Omega_1 e^{i(\omega_1 - \omega_{ac})t} c_a \quad (8)$$

To find the condition for EIT, we must find the condition where $\frac{\partial}{\partial t} c_a$ is equal to zero. This means that no atoms are moved to the excited state. The resulting equation is shown below.

$$\Omega_1 c_b = -\Omega_2 c_c e^{i[(\omega_2 - \omega_{ac}) - (\omega_1 - \omega_{ab})]t} \quad (9)$$

The equation above gives two conditions. First, the difference in laser frequencies, $\omega_1 - \omega_2$, must be equal to the differences in the energies of levels b and c, ω_{bc} . This condition is called a two-photon resonance, and implies that no atoms in the ground states b and c will be excited into state a, thus achieving EIT. Second, the requirement of the population distribution becomes, $\Omega_1 c_b = -\Omega_2 c_c$. Now, solving for the coefficients, c_a , c_b , and c_c with the new condition for EIT, we find.

$$|D\rangle = \frac{\Omega_2 e^{-i\omega_b t} \psi_b - \Omega_1 e^{-i\omega_c t} \psi_c}{\sqrt{\Omega_1^2 + \Omega_2^2}} \quad (10)$$

This quantum state, which does not interact with the incident laser is called the dark state, i.e. $\hat{H}|D\rangle = 0$. There is an orthogonal quantum state $|B\rangle$ which is the bright state and fully interacts with the laser. When an atom is in the dark state, there it will remain.

So far, this whole derivation has neglected the effects of spontaneous emission of the three level atom. In fact, spontaneous emission is one of the most important aspects of EIT resonances which requires a more formal density matrix treatment of the subject which considers the contribution of the vacuum EM field to spontaneous emission [8]. If an atom becomes moved to the excited state, $|a\rangle$, it will again decay to a metastable state, either finding its way to the bright state or the dark state. If it lands in the dark state, there it will remain. However, if it is in the bright state, it can be excited to state $|a\rangle$ again, where it will again spontaneously decay into either the bright state or the dark state. This optical pumping will eventually transport the entire electron population to the dark state. Because of this, when we interrogate a Λ configuration with lasers at a two photon resonance, $\omega_1 - \omega_2 = \omega_{bc}$, the medium becomes transparent.

Since the goal of this project is to measure Zeeman shifts in the atom's energy levels and changes in the atom's orientation, we can apply the laser fields, E_1 and E_2 scan their two-photon detuning to probe the EIT resonance. The width of transmission resonances, with low laser power, can be as narrow as tens of Hz. This allows for the superb sensitivity of the EIT magnetometer.

2.3 EIT in ^{87}Rb

All of the preceding theory related to a general three level Λ -system. However, the EIT magnetometer uses ^{87}Rb atoms with more complicated level structure shown in figure 3. We use the D1 transition in Rb and find that there are actually many possible Λ -systems shown in figure 3. Each of the lower levels has a Zeeman shift

amplitude of $.7 \text{ MHz/Gauss}\cdot m$. As a result the two ground states, $F=1,2$, consist of three and five Zeeman sublevels respectively. When a magnetic field is applied, multiple EIT resonance occurs at up to seven different two-photon detunings. We label the corresponding EIT peaks a_{-3} through a_{+3} . When the magnetic field is zero, the Zeeman shift becomes zero and the transitions are all at degenerate energies. This easily provides a very accurate method for deducing the strength of the magnetic field due to the narrow EIT peaks. We have found that our apparatus can measure changes of $.1\text{Hz}$ in two-photon detuning which means we can measure magnetic fields as small as 10pT . [9]

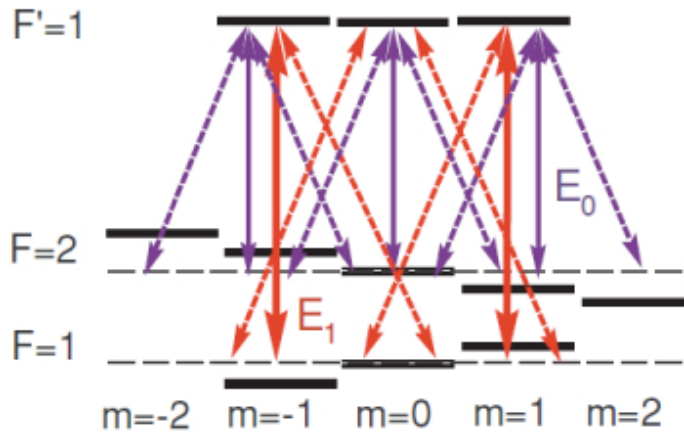


Figure 3: Multiple Λ -systems in ^{87}Rb .

For the EIT magnetometer we use two linearly polarized laser fields. Alternate approaches can be implemented using circular polarization, but these systems have one drawback. Circularly polarized light drives no transitions from the $F = 2$ to $F' = 1$, $m = \pm 2$ transitions and either the $F = 2$ to $F' = 1$, $m = +1$ or $F = 2$ to $F' = 1$, $m = -1$ transitions depending on polarization rotation direction. In the process of optical pumping, instead of being pumped into the dark state, electron population will be trapped in these sublevels, uncoupled to the laser field. Unfortunately, while atoms in a dark state are sensitive to the laser's two-photon detuning, resulting in

narrow EIT resonances, atoms trapped in these uncoupled quantum states will never interact with either laser field, giving no EIT signal. In this case, the final result with circular polarization is that at any given time during measurements of EIT, many atoms will become useless for measuring EIT resonances, resulting in a loss of signal. This is one strong motivation for using linearly polarized light, where an atom in any Rb ground state sublevel can become excited.

The level structure in Rb containing many EIT Λ -systems also requires a detailed theoretical treatment of EIT for the entire system. When an atom is excited into an F' state, it can decay into an adjacent energy level which is part of a different Λ -system. In this case, we cannot theoretically treat each EIT system independently, but must consider the Clepsh Gordon coefficients for in Rb to deduce the amplitude of each resonance. This work was done by theory collaborators at Novosibirsk State University, Russia, and can be seen later in matching experimental and theoretical plots of EIT amplitude heights.

3 Experimental Setup

3.1 Overview

The experimental setup for the EIT magnetometer is shown in figure 4. A frequency modulated Vertical Cavity Surface Emitting Laser (VCSEL) with linear polarization passes through a cylindrical rubidium vapor cell (diameter = 22mm, length = 75mm) containing isotopically enriched ^{87}Rb and 15 Torr of Ne buffer gas housed inside a magnetic shield. The laser is frequency stabilized to 795nm using a Dichroic Atomic Vapor Laser Lock (DAVLL). Also, the laser polarization is controlled by a polarizing beam splitter (PBS) and a $\lambda/2$ waveplate before the rubidium cell. After the cell, the laser transmission is measured and imported into the homemade computer data acquisition system which also controls the modulation frequency of the laser. By

manipulating the laser polarization, and changing the laser modulation frequency and thus the two-photon detuning, we can scan multiple narrow EIT resonances in rubidium vapor. The transmission resonances are then recorded and analyzed in order to deduce information about the magnetic field direction.

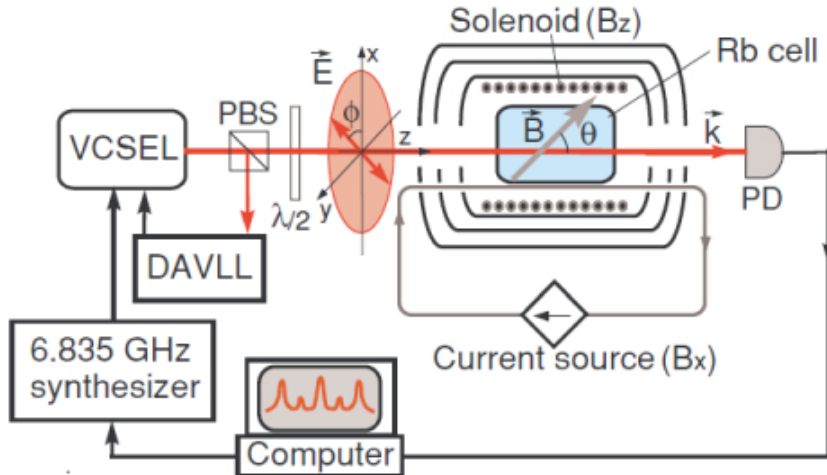


Figure 4: Experimental setup.

3.2 Vertical Cavity Surface Emitting Laser

EIT requires two laser fields coupled to a 3-level Λ -system. To scan narrow resonances, the two-photon detuning between the two laser fields must be precisely controlled and the phase of the laser fields must match. However, lasers available for this use only have a stabilization near 1MHz, making the task of measuring EIT resonances impossible with two different lasers. Instead, we use a single frequency laser modulated at 6.835GHz and controlled by a homemade computer-controlled microwave source. The frequency modulation of the laser field produces discrete frequency components separated in Fourier space by the modulation frequency. In this case, even if the laser's frequency is unstable, the two-photon detuning between the carrier and sidebands remains constant, allowing us to scan narrow resonances with widths below 100 Hz. Using this modulation and the DAVLL, we tune the optical carrier frequency to the

$F=1$ to $F'=1$ transition and the first order sideband to the $F=2$ to $F'=1$ transition. We control the amplitude of the modulation signal so that the intensity ratio of the first modulation sideband to carrier is 60%. This is a ratio that allows the cancellation of resonance shift dependence on laser amplitude to first-order in the setup [5].

To achieve this microwave frequency tunability we use a VCSEL. Due to its tunability, low power consumption and small size, the VCSEL is the laser commonly used for miniature atomic clock and magnetometer experiments [4]. Inside the VCSEL operation range, the VCSEL frequency depends linearly on the current applied to the laser. Another property of the VCSEL is frequency dependence on temperature, $.6\text{nm}/^\circ\text{C}$. This dependence allows us to adjust the frequency of operation of the laser but also requires us to control the temperature of the laser with precision below $.1^\circ\text{C}$. Applying a laser current of 1.6mA, we conducted our experiment with laser powers from $50\mu\text{W}$ to $250\mu\text{W}$; the high power allows for a clean signal, but the low power allowing for narrower resonances.

3.3 Dichroic Atomic Vapor Laser Lock

To access the individual ^{87}Rb hyperfine sublevels in the D1 transition using the EIT scheme, the laser's frequency stabilization must be locked to the D1 transition frequency. For this reason, we need to use an effective laser lock which can tune the laser frequency to the D1 transition of rubidium. There is also another requirement of our laser lock. To create the two laser fields needed for EIT, we must modulate the laser to create discrete frequency components with spacing equal to the hyperfine splitting in ^{87}Rb (6.835 GHz). Therefore, while many frequency stabilization methods require a modulated laser to achieve a steep error signal, it is much simpler for us to use an unmodulated laser stabilization method and not add additional modulation to the laser. Given these concerns, the most effective choice for laser stabilization is the Dichroic Atomic Vapor Laser Lock (DAVLL). This scheme uses a schematic shown

below in figure 5. A linearly polarized laser, roughly tuned to the D1 transition in rubidium, travels through a vapor cell with a magnetic field in the propagation direction. After the cell, the laser passes through a $\lambda/4$ waveplate followed by a polarizing beam splitter (PBS) and the signals are detected and subtracted from one another. This creates an error signal with a zero crossing point at the frequency of the D1 transition. The explanation of this error signal is as follows.

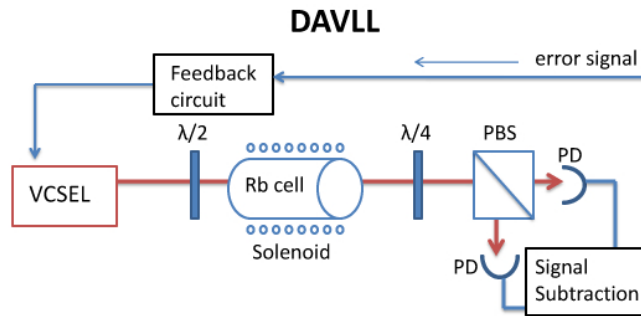


Figure 5: Experimental setup of the DAVLL.

The incoming linearly polarized laser can be decomposed into two laser fields with opposite circular polarization. Passing through the vapor cell, the laser will undergo Doppler-broadened absorption as it passes through the cell. If no magnetic field were applied, the Zeeman sublevels ($m = 1$ and $m = -1$) would be degenerate and the two circularly polarized laser fields would be equally absorbed. However, when the magnetic field is applied, the $m = -1$ and $m = 1$ transition are Zeeman shifted. Now, each of the opposite handed circularly polarized fields only makes transitions from either the $m = 1$ or the $m = -1$ state. Therefore, the center of the absorption peak is frequency shifted for each field. Each of these absorption signals, once sent through the $\lambda/4$ waveplate, are then separated by the PBS and sent to independent detector arms. Subtraction of the Doppler-broadened absorption peaks at slightly different frequencies explains the dispersion-shaped error signal centered around the desired Rb resonance. We use this error signal to frequency stabilize the laser at

the desired transition. Below is a figure showing the DAVLL lock signal using a 6.385GHz modulated laser shown on the same graph with the Doppler-broadened absorption spectrum of ^{87}Rb . By locking to the point indicated on the graph, we achieve the necessary long term stability.

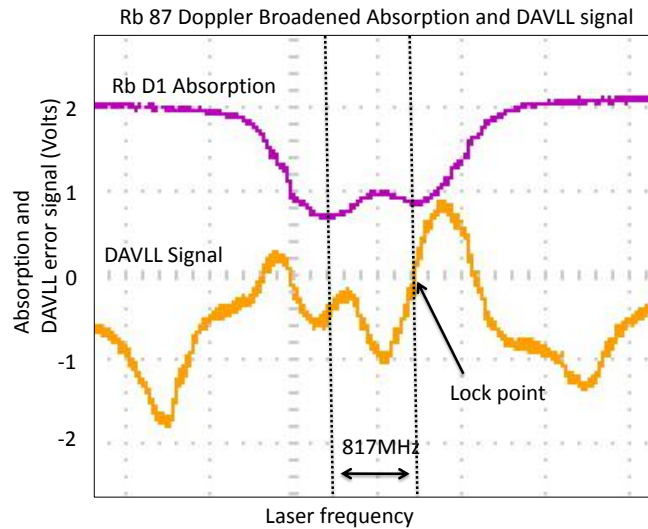


Figure 6: DAVLL error signal (yellow), and Doppler broadened absorption (purple) for the rubidium D1 line with a 6.385 GHz frequency modulated laser.

There are more important experimental details regarding the DAVLL lock which effect the shape, slope, and offset of the error signal. First, the strength of the magnetic field changes the amplitude, slope, and zero-crossing of the DAVLL signal. The optimal Zeeman splitting created by the magnetic field should be nearly the same as the width of the Doppler broadened absorption line. We created this magnetic field with permanent magnets arranged around the cell. Another important experimental parameter is the temperature of the rubidium cell. By increasing the temperature of the atoms, a better error signal can be created since the vapor density of the atoms increases. The last, and most important, experimental parameter for the DAVLL

signal is linear polarization. Changing the $\lambda/4$ polarization of the laser after the Rb cell is the easiest way to change the offset of the error signal and therefore the frequency of the lock. Simply put, changing this angle creates an imbalance between the signals which are sent to each detector arm, and therefore the signal offset is shifted. Since the purity of the EIT resonances we study is dependent on laser frequency (one-photon detuning), we must be able to control the single-photon detuning using the $\lambda/4$ polarizer.

3.4 Controlling the Magnetic Field

The magnetic shield around the Rb vapor cell consists of a three-layer μ -metal shield. A solenoid inside the cell creates a magnetic field in the longitudinal direction. Also, a wire parallel to the beam line provides a vertical magnetic field along the laser beam (see figure 4). By inversely varying the field created by the solenoid and the wire, we produce magnetic fields of uniform strength over the line of laser propagation, but with different direction. However, since the strength of the magnetic field from the wire varies as inverse distance, the vertical component of the magnetic field is not constant over the width of the laser beam. Since our laser beam only had a width on the order of 1mm, and the laser was detected by a photodetector which averages over the whole signal, we originally conducted the experiment on the assumption that the wire's magnetic field is constant in magnitude and direction in the vertical plane. However, theoretical work showed that this inhomogeneous magnetic field broadened the EIT resonances and affected their relative amplitudes. For this reason, the inhomogeneity was taken into account when the theoretical numerical calculations were made. Lastly, the rubidium cell is held in place and heated by a copper mount attached to a resistive heater. This heats the cell to a stable temperature of $47.3^{\circ}C$, increasing the vapor pressure of the rubidium cell for an increased number of atoms interacting with the beam.

4 Measuring Magnetic Field Direction

The two applied lasers address every EIT system in Rb, corresponding to resonances at up to seven non-degenerate two-photon detunings in the presence of a magnetic field. The amplitudes of these resonances are strongly dependent upon the orientation of the magnetic field and laser polarization. In fact, due to the selection rules, for special orientations of the electric field $\vec{E} \perp \vec{B}$ and $\vec{E} \parallel \vec{B}$, certain transitions are not allowed causing less than seven of the EIT resonances to exist. One recent proposal [10] as well as our experiment and the corresponding theory show that for all orientations of the magnetic field, absolute minima and maxima exist for the amplitude of every EIT resonance when the electric field (laser polarization) lies in the plane created by the magnetic field and the laser propagation direction (wave vector, \vec{k}); that is $E \parallel (\alpha \vec{B} + \beta \vec{k})$, where α and β are arbitrary constants. By controlling the linear polarization for the incoming lasers, the selection rules dictate which transitions are allowed. Figure 7 below shows various orientations of the magnetic field and laser polarization and the corresponding angles in a cartoon Rb vapor cell. The magnetic field direction defines the z-axis for the atoms.

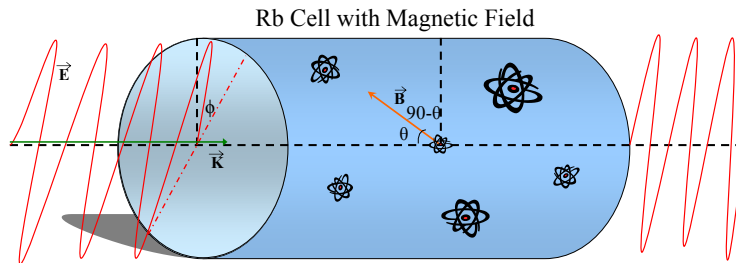


Figure 7: Rb Cell with electric and magnetic field orientation angles ϕ and θ .

As mentioned earlier, for general orientations of the electric field and magnetic field, EIT resonances at seven two-photon detunings are allowed. For convenience, we label the corresponding EIT transmission peaks a_{-3} , a_{-2} , a_{-1} ... a_3 . For these data sets we apply a magnetic field of uniform strength so that the Zeeman splitting between EIT peaks was 25kHz. This made curve-fitting and data analysis more convenient.

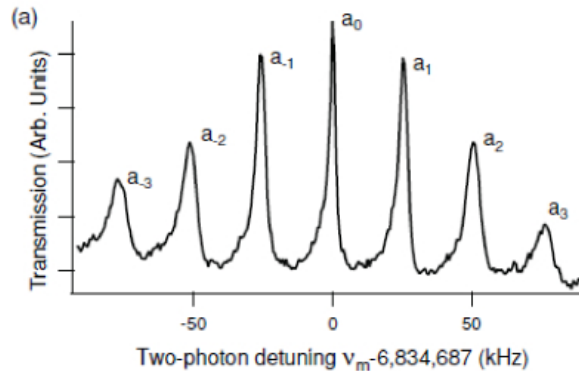


Figure 7: Example of seven EIT resonances with for angles $\theta = 90^\circ$ and $\phi = 60^\circ$

4.1 Special Cases

For special cases of magnetic field and polarization the resulting EIT resonances are very simple understand to and give an idea of how the EIT magnetometer is sensitive to magnetic field direction. Two special cases will be addressed. First, consider the case of $\phi = 0^\circ$ and $\theta = 90^\circ$ (light polarization parallel to magnetic field). In this case, selection rules only allow transitions with $\Delta m = 1$, and the dotted line transitions in figure 3 are not allowed. The derivation for this selection rule is easy, and a clever use of the commutation relations [7]. The transition probability is related to the value of the matrix element $\langle \psi_{m'} | \hat{p} | \psi_m \rangle$, where \hat{p} is the polarization direction. For $\hat{p} = \hat{z}$, we use the commutation relation $[F_z, z] = 0$, which gives:

$$0 = \langle \psi_{m'} | [F_z, z] | \psi_m \rangle = \langle \psi_{m'} | F_z z - z F_z | \psi_m \rangle = (m' - m) \hbar \langle \psi_{m'} | z | \psi_m \rangle \quad (11)$$

Therefore, either $m = m'$, or $\langle \psi_{m'} | \hat{p} | \psi_m \rangle$ is zero, and no transitions can occur. Furthermore, the transition from $F = 1$ to $F' = 1$ with $m = 0$ is also forbidden due to conservation of momentum, so only two EIT resonances occur as shown in figure 8.

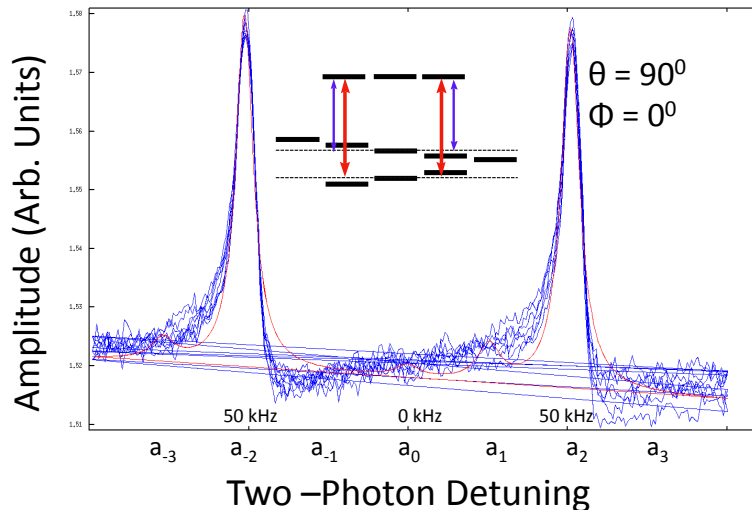


Figure 8: EIT spectrum and corresponding ^{87}Rb transitions for transverse magnetic field, $\theta = 90^\circ$, with $\phi = 0^\circ$

The second special case is a transverse magnetic $\theta = 0^\circ$. In this situation the z-direction of the aligned atoms points directly into or away from the laser propagation direction. This configuration is symmetric under polarization rotation, so it is intuitive that EIT resonances will not depend on the polarization angle, ϕ . The selection rules for this setup allow only transition of $\Delta m = 1$, allowing three EIT resonances, a_0 , a_2 , and a_{-2} . Notice, the a_2 , and a_{-2} EIT peak occur with both transitions $\Delta m = 0$ and $\Delta m = 1$. This is because there are multiple Λ -systems with the a_2 , and a_{-2} two-photon detuning. This special case is shown in figure 9. Due to symmetry, similar spectra are observed $\theta = 90^\circ$ and $\phi = 90^\circ$.

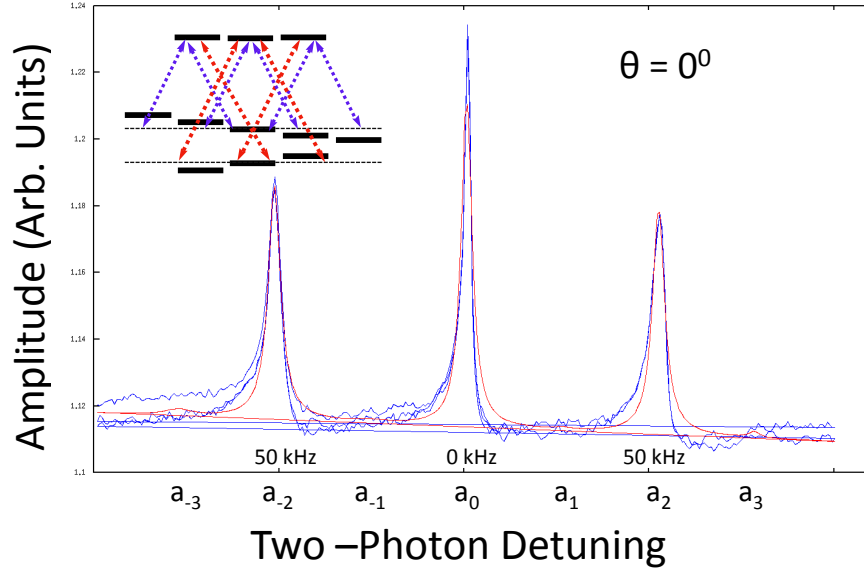


Figure 9: EIT spectrum for a longitudinal magnetic field ($\theta = 0^\circ$).

These two special cases show that the EIT magnetometer can be used to determine the orientation of the polarization vector with the magnetic field vector. Finding the magnetic field with special cases is easy. For $\theta = 90^\circ$ or $\theta = 0^\circ$ you can rotate the linear polarization until you find a case where polarization, \vec{E} , is perpendicular or parallel to \vec{B} . Many EIT peaks will go to zero, and you can know the direction of the magnetic field. However, we have confirmed that it is possible to determine magnetic field directions which are not parallel or orthogonal to \vec{E} . However, the fact that the case with $\theta = 90^\circ$ $\phi = 90^\circ$ and $\theta = 0^\circ$ are give similar-looking EIT pictures highlights the fact that a single measurement is not enough to fully determine the magnetic field. This will be expounded upon in the next section.

4.2 Universal EIT Maxima and Minima

In the previous section, I argued that for longitudinal magnetic fields, EIT amplitudes are independent of laser polarization. For transverse magnetic fields, the opposite is

true. The special cases, considered above, show that for a transverse magnetic field, EIT transmission peaks can oscillate from zero amplitude up to their maximum. To show this, we construct plots of EIT peak amplitude as a function of polarization for each of the seven EIT peaks. For $\theta = 90^\circ$, the plot is shown in figure 10. This experimental data is interesting because, while it represents the special cases at angles with θ and ϕ equal to 90° or 0° , it also displays behavior which has not been explained hitherto and in fact cannot be derived without the more rigorous approach mentioned earlier. For instance, while every EIT peak has either a maximum or minimum at the laser polarization mentioned earlier, several EIT amplitudes have maxima and minima at intermediate locations which do not occur at identical frequencies. While the $a_{\pm 2}$ and $a_{\pm 1}$ peaks have max and min close to $\phi = 45^\circ$, the $a_{\pm 3}$ are at a slightly lower frequency and a_0 does not have a max or min around 45° . In fact, only “universal” (not depending on experimental parameters) maxima and minima are found. Universal maxima and minima, which do not depend on experimental parameters, can only be found based on the condition that \vec{E} is perpendicular to the $\vec{B} - \vec{k}$ plane.

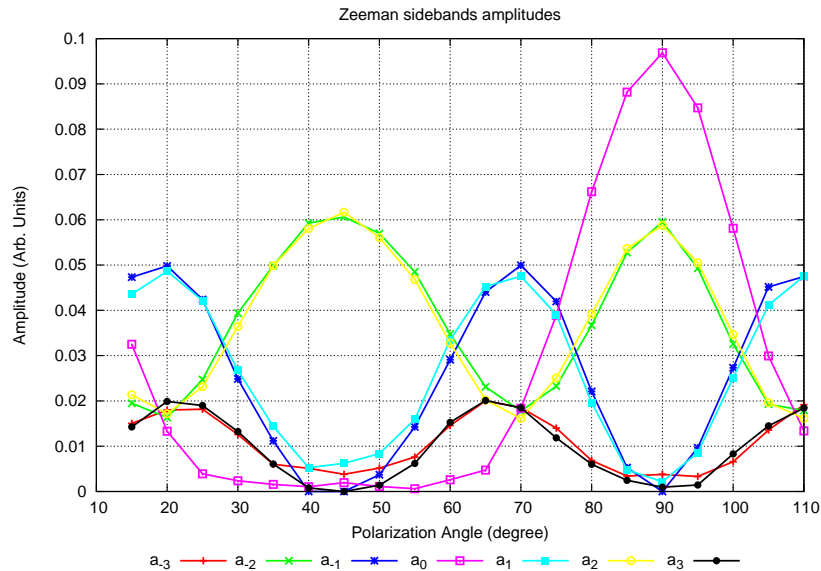


Figure 10: EIT peak amplitude as a function of angle for $\theta = 90^\circ$

From the previous section, I argued that EIT amplitudes should not depend on polarization for longitudinal magnetic field ($\theta = 0$). The experimental data for this is shown in figure 11.

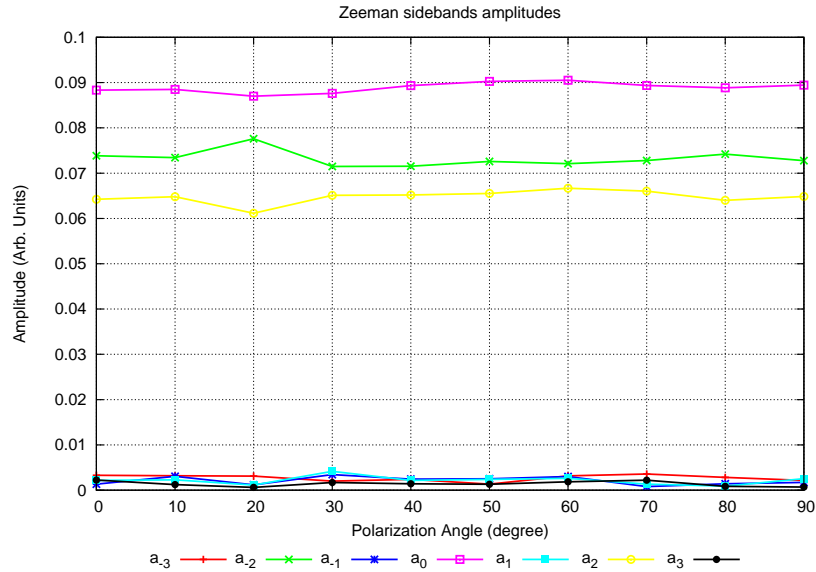
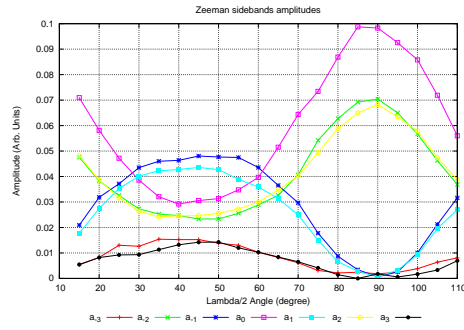


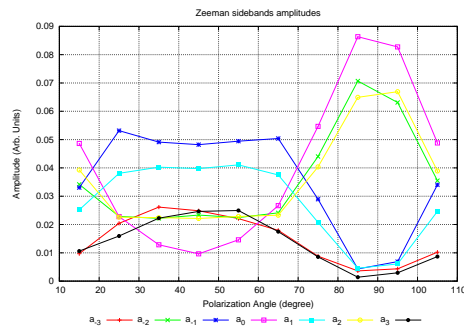
Figure 11: EIT peak amplitude as a function of angle for $\theta = 0^\circ$

What happens then, for the intermediate and general case when the magnetic field is arbitrary, θ between 0° and 90° ? In this case, some component of the atoms' orientation, \vec{z} is in the laser propagation direction \vec{k} and another component is orthogonal. EIT peak amplitude fluctuates strongly with polarization angle for transverse fields, and is independent for longitudinal fields. It is expected, then, as θ increases, that the dependence on laser polarization will decrease. However, the universal maxima and minima should still exist until the transverse component of the magnetic field goes to zero. This is experimentally observed. Figure 12 is a plot of EIT amplitude versus laser polarization for magnetic field angles of $\theta = 15^\circ$, $\theta = 45^\circ$, and $\theta = 75^\circ$.

a)



b)



c)

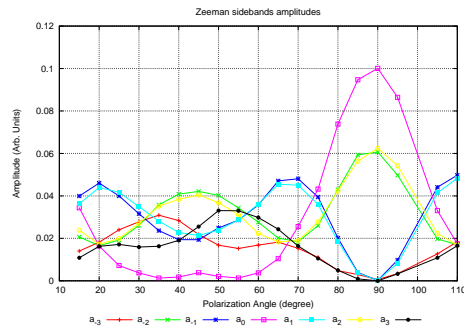


Figure 12: EIT amplitude as a function of polarization angle ϕ for a) $\theta = 15$, b) $\theta = 45$, and c) $\theta = 75$.

While each of these graphs demonstrate interesting behavior for the non-universal EIT maxima and minima, they confirm the predicted behavior of a decrease in dependence on polarization angle as the magnetic field becomes perpendicular to laser transmission at 180° and 90° . Also, the “universal” maxima and minima, while less

sharply peaked, are consistently evident for all magnetic fields which are not parallel. Furthermore, opposite EIT peaks (i.e. ± 1 , show different behavior. Ideally, opposite peaks should demonstrate symmetric behavior, but the hyperfine structure of the excited state causes a dependence of the EIT system on one-photon detuning. For measuring small magnetic fields this causes the observed assymetry.

Additionally, an elliptically polarized laser beam can also create assymmetric EIT spectra. This effect is quite convenient since it allows the determination of the overall sign of the magnetic field. If the magnetic field is positive along the laser propagation direction with right-handed polarization, the positive EIT peaks will be larger.

In conclusion, the data in figure 12 shows that by rotating laser polarization, the angle of universal minima and maxima can be found. This angle corresponds to an angle that lies in the plane created by the magnetic field vector \vec{B} and the laser propagation direction, wave vector \vec{k} . To find the absolute direction of the magnetic field more information is needed. There is more than one way to gain this information. One way is to add a known magnetic field to that measured and take the measurement again, finding a new plane created by \vec{k} and \vec{B}' , then calculating the intersection of these two planes. Another method is to use a laser traversing the Rb cell in an orthogonal direction, and combine the two measurements. Lastly, a third way is to compare the amplitudes of the EIT peaks to one another. Figure 12 demonstrates that the relative amplitude of each EIT peak is dependent on the angle θ . By calibrating a setup with known magnetic fields for these values, the total magnetic field could be determined simply by observing the ratio of peak heights in a single measurement. However, it is also true that peak ratios are dependent upon other experimental parameters such as laser intensity, Rb vapor pressure, and so on. Therefore, in order to use this method the setup would need to be well calibrated.

4.3 Comparison with Theory

For magnetic field angles of $\theta = 90^\circ$ and $\theta = 15^\circ$, we have theoretical plots to accompany and confirm the experimental results. The numerical calculations were made using the density matrix approach [8] assuming low saturation and complete depolarization of the excited state for collisions. The laser intensities and all other parameters used matched the experimental conditions. In order to achieve the good agreement, we had to include the effects of the non-homogeneous magnetic field from the parallel wire and average the calculations over a twenty-five point grid.

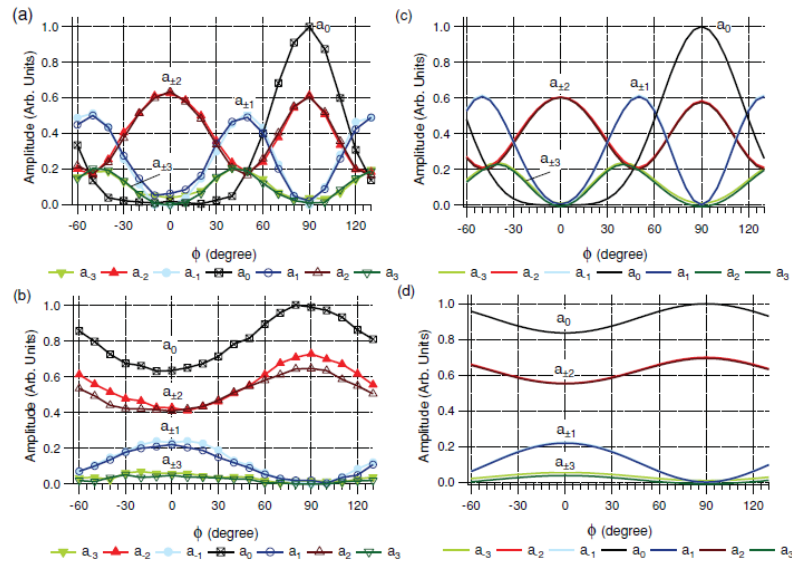


Figure 13: a & b) Experimental plots and c & d) Theoretical calculation for EIT amplitudes versus polarization angle, ϕ for a & c) $\theta = 90$ and b & d) $\theta = 15$

5 Effects of Elliptical Polarization on EIT

In any experiment, a linearly polarized laser will have a small amount of ellipticity. For this reason, we have studied the effects of elliptical polarization on the EIT magnetometer. In some ways a small elliptical polarization might skew the results of

the magnetometer and need to be well understood so that errors aren't introduced. However, we also found that elliptical polarization can help reduce some degeneracies in the system to give a more complete measurement of magnetic field direction. For example, one challenge in finding the direction of the magnetic field with the EIT magnetometer is finding the overall sign of the magnetic field. One way to do this is by applying a small elliptical polarization to the setup. Circularly polarized light behaves differently with the ^{87}Rb Λ -systems than linearly polarized light. The allowed Λ -systems are shown below.

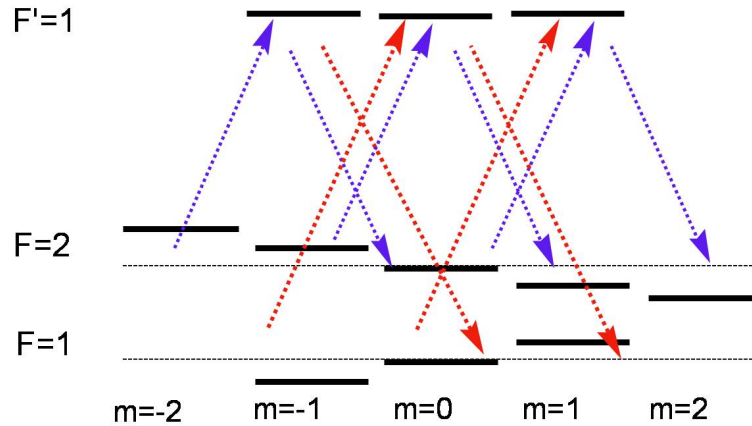


Figure 14: Allowed transition for right-handed circularly polarized light on ^{87}Rb .

In this new system, the transmission peaks are dependent on the positive or negative orientation of the magnetic field. Therefore, adding a small circular polarization to the experiment and observing the asymmetric EIT peaks is one way to determine the overall sign of the magnetic field.

5.1 EIT Shifts from Elliptical Polarization

We studied the effects of elliptical polarization of the linear polarization at which we find universal EIT maxima and minima. This is an effect which, if found to be large, could become an annoyance for the accuracy of the magnetic compass. While current

theory indicates that in an ideal EIT system no shifts in EIT maxima and minima should occur, we have measured a linearly shift with elliptical polarization. To make this measurement, we rotated the polarization angle, ϕ , to make plots similar to those shown in figure 12. We then changed the ellipticity of the polarization with a $\lambda/4$ waveplate and took the same data for different ellipticities. Comparing these plots, we graphed the polarization of universal EIT maxima and minima verses ellipticity.

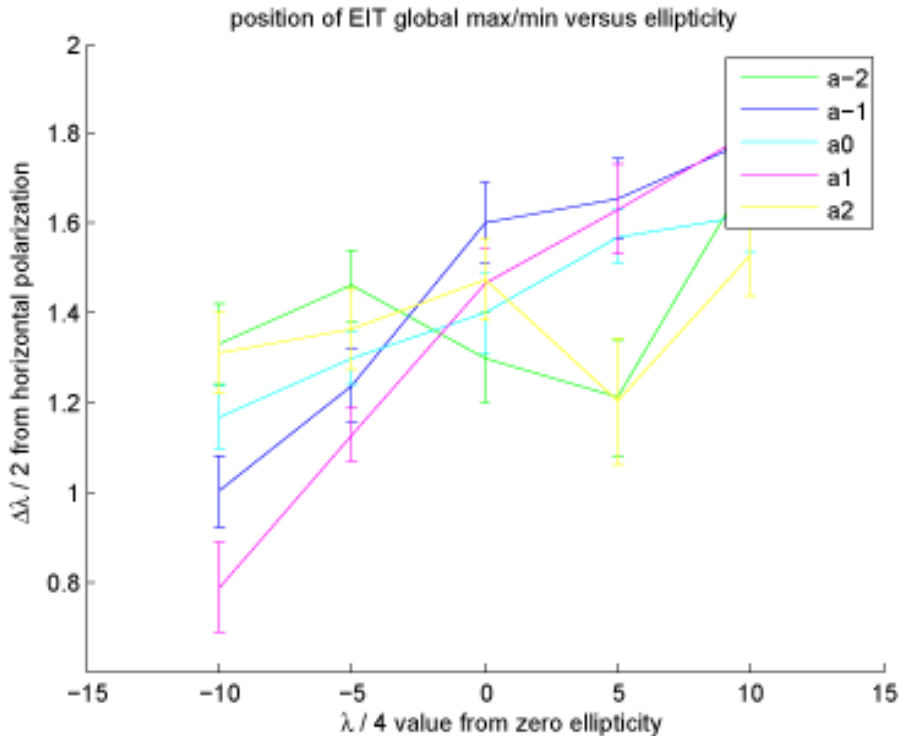


Figure 15: Measurement of EIT global maxima and minima polarization as a function of ellipticity

This data showed a somewhat linear shift for all five EIT resonances, but was noisy and somewhat inconclusive (data for $a_{\pm 3}$ peaks not displayed due to too much noise). We then developed another, simpler measurement technique. To find the polarization of the EIT max and min for each ellipticity, I simply rotated the $\lambda/2$ polarizer and manually watched for polarizations where the a_1 or a_{-1} peak had a minimum. I then changed the elliptical polarization and made this measurement again, correcting the linear polarization value for the rotation added by the $\lambda/4$ waveplate. The results of

this experiment are shown below, and show agreeing data which is less noisy. Overall, while the linear shifts seem to be evident, the slope is small. Since theory does not predict these shifts, the cause is ultimately unknown, but might be due to some experimental characteristic of the setup.

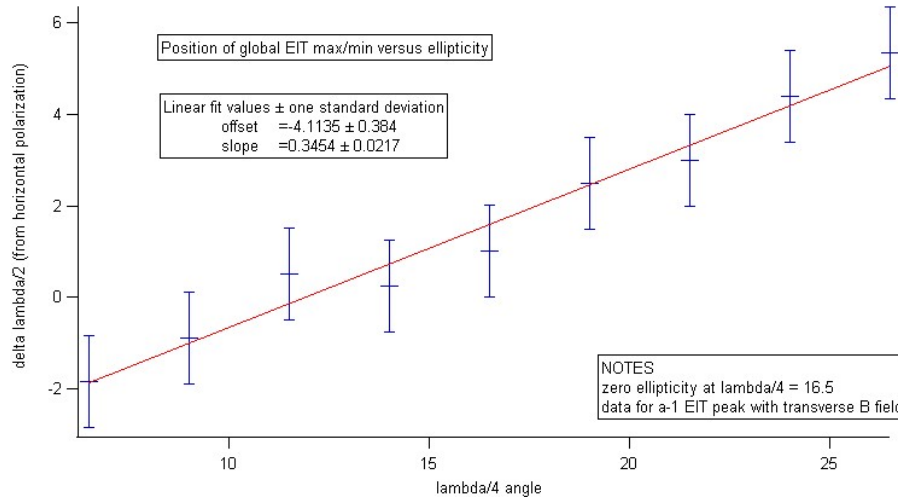


Figure 16: Shift of EIT global maxima and minima as a function of ellipticity.

6 Future Prospectives

One of the main advantages of the EIT magnetometer scheme is the capability of creating complete three-dimensional vector field maps of magnetic fields. To do this, we would place a multi-pixel camera in place of the photodetector used for the standard setup. In this case, measurements of EIT maxima and minima could be taken at every pixel. Using one laser, this method could give a two-dimensional map. However, by using a second laser propagating through the Rb cell in a perpendicular direction, the extra information could be obtained. However, for this measurement to become accurate, a thin Rb cell should be used so that the magnetic field is not averaged over long distances. On this topic, the two-dimensional scalar magnetic field map has already been demonstrated [11]. The two-dimensional vector field map measurement is the next ongoing project in this research.

7 Conclusion

In the past, setups similar to the EIT magnetometer have been utilized for prototype miniature atomic clocks. From these experiments it has become clear that transitions in ^{87}Rb can be very precisely measured down to .1Hz [9]. From such an experiment run with the exact setup used for this experiment, we know that the sensitivity of the EIT magnetometer to the magnitude of magnetic fields is competitive with some of the best magnetometers in use today. Much of the effort in my project has been focused towards the added capability of measuring magnetic field direction. This is the capability which sets the EIT magnetometer apart from other similar devices and makes interesting applications possible such as mapping both the strength of electrical currents in human organs including the heart and brain. We have shown that complete magnetic field direction measurement takes more than a single measurement, but is possible by various methods. While elliptical laser polarizations can be used to increase the useful information in the measurements, the position of universal minima and maxima depend linearly polarization ellipticity. This is an effect which has not been showed by any previous experiment. The current and future thrust of EIT magnetometer research is to put every facet of research to completion and demonstrate multi-dimensional mapping by using multiple lasers, CCD cameras, and possibly retro-reflected lasers to create complete field maps of regions in space.

References

- [1] J. Clarke, “SQUID Sensors: Fundamentals, Fabrication, and Applications”, edited by H. Weinstock (Kluwer Academic, The Netherlands, 1996), pp. 1–62.
- [2] I. K. Kominis, T. W. Kornack, J. C. Allred, and M. V. Romalis, “A subfemtotesla multichannel atomic magnetometer” *Nature (London)* **422**, 596 (2003).

- [3] V. Shah, S. Knappe, P. D. D. Schwindt, and J. Kitching, “Subpicotesla atomic magnetometry with a microfabricated vapour cell”, *Nature Photonics* **1**, 649 (2007).
- [4] J. Vanier, “Atomic clocks based on coherent population trapping: A review”, *Appl. Phys. B* **81**, 421-442 (2005).
- [5] N. Belcher, E. E. Mikhailov, and I. Novikova, “Atomic clocks and coherent population trapping: Experiments for undergraduate laboratories”, *Am. J. Phys.* **77**, 988 (2009).
- [6] K. Cox, V. I. Yudin, A. V. Taichenachev, I. Novikova, and E. E. Mikhailov, “Measurements of the magnetic field vector using multiple electromagnetically induced transparency resonances in Rb vapor,” *Phys. Rev. A* **83**, 015801 (2011).
- [7] D. J. Griffiths, *Introduction to Quantum Mechanics*, 2nd ed. Pearson Prentice Hall, Upper Saddle River, NJ, (2005).
- [8] A. V. Taichenachev, V. I. Yudin, R. Wynands, M. Stahler, J. Kitching, and L. Hollberg, “Coherent-population-trapping resonances with linearly polarized light for all-optical miniature atomic clocks”, *Phys. Rev. A* **67**, 033810 (2003).
- [9] E. E. Mikhailov, T. Horrom, N. Belcher, and I. Novikova, “Performance of a prototype atomic clock based on $lin||lin$ coherent population trapping resonances in Rb atomic vapor”, *J. Am. Opt. Soc. B* **27**, 417 (2010).
- [10] V. I. Yudin, A. V. Taichenachev, Y. O. Dudin, V. L. Velichansky, A. S. Zibrov, and S. A. Zibrov, “All-optical compass based on the effect of electromagnetically induced transparency”, *Phys. Rev. A* **82**, 033807 (2010).

- [11] E. E. Mikhailov, I. Novikova, M. D. Havey, and F. A. Narducci, “Magnetic field imaging with atomic Rb vapor”, *Optics Letters*, Issue 22, 34, 3529-3531, (2009).
Opt. Lett. **34**, 3529 (2009).